RSC Advances

PAPER

View Article Online
View Journal | View Issue

Cite this: *RSC Adv.*, 2015, **5**, 33185

Oxidative coupling of 2-naphthol to (*R*)/(*S*)-BINOL by MCM-41 supported Mn-chiral Schiff base complexes†

Kusum K. Bania,*[a] G. V. Karunakar[b] and Lanka Satyanarayana[c]

Received 26th February 2015
Accepted 31st March 2015

DOI: 10.1039/c5ra03492b

www.rsc.org/advances

Three Mn(III)-chiral Schiff base complexes supported on MCM-41 are found to be effective reusable catalysts for enantioselective oxidation of 2-naphthol to (*R*)- and (*S*)-BINOL (1,1′ bi-2-naphthol) in the presence of oxygen. The supported Mn(III)-complexes are characterized by PXRD, FTIR, solid state-NMR, BET, and cyclic voltammetry study. The homo-coupling reaction with oxygen as the oxidant is promoted by 20 mg of Mn(III) Schiff base complexes to afford binaphthols in nearly quantitative yields with high enantioselectivity of up to 91% ee. The catalytic activities of the homogeneous and heterogeneous chiral catalyst are found to be almost similar. However, the heterogeneous counterparts are found to be advantageous in terms of recyclability and storability. Oxygen partial pressure, the nature of the solvent, temperature and the amount of catalyst affect the catalytic oxidation process. High temperature and highly polar solvent are found to have adverse effects on the catalytic oxidation process.

1. Introduction

Activation of the C–H bond *via* oxidative coupling reaction has been a long standing goal in the field of chemical research.[1–3] Out of the various oxidative coupling reactions, the oxidative coupling of 2-naphthol to axially chiral *C*2-symmetric 1,1′ bi-2-naphthol (BINOL) is considered to be one of the most versatile organic transformations.[4,5] Chiral BINOL and its derivatives are found to act as chiral auxiliaries and ligands in asymmetric transformations.[6–8] They also serves as backbone for various biologically active natural products such as bioxanthracene (−)-ES-242-4, cercosporin and calphostins A–D.[9] Because of these importance of such molecule has fuelled the researchers to develop efficient methodology and chiral catalyst for asymmetric coupling of 2-naphthol. Subsequently many homogeneous[10,11] and heterogeneous chiral catalysts[12,13] have been reported to catalyze such reaction with moderate to high yield and enantioselectivity. Chiral Schiff base complexes of iron (Fe),[14,15] ruthenium (Ru)[16] and vanadium(v) appears to be promising catalyst.[17,18]

Although the homogeneous catalyst are found to have better catalytic activity but they fails in terms of recovery and reusability.[19] Since chiral catalysts are costly so it is equally important to restore the catalytic activity for longer period of time and also enhanced their recyclability.[20] In current development of heterogenisation of homogeneous catalyst inorganic materials like MCM-41, zeolites, LDHs, silica[21–23] *etc.* plays a pivotal role in designing of chiral heterogeneous catalyst. However, a limited number of heterogeneous chiral Schiff base complexes have been developed for such asymmetric oxidative reaction. Very recently, chiral self-dimerized vanadium complexes on SiO_2 were developed for the oxidative coupling of 2-naphthols with a maximum enantioselectivity of 90% ee.[24,25] From our group we report for enantioselective oxidation of 2-naphthol *via* cation–π interaction in presence of zeolite-Y supported Fe-Schiff base complexes and also by trinuclear Fe-oxo carboxylates.[23,26]

Out of the various inorganic mantles MCM-41 has as well-ordered pore arrays, large surface area, uniform pore size distributions and tunable pore diameter (4–15 nm).[27] Because of these unique properties MCM-41 has been extensively used for immobilization of chiral metal catalyst.[28,29] So in order to develop efficient and recyclable chiral catalyst in this report we examined the catalytic activity of three chiral Mn(III)-Schiff base complex supported on MCM-41. The heterogeneous chiral catalyst is found to be efficient catalyst for oxidative coupling of 2-naphthol in terms of yield and enantioselectivity. Prior to this, these catalysts are recycled for three consecutive cycles without any deactivation.

2. Experimental method

2.1. Materials and physical measurements

Hexagonal siliceous MCM-41 is purchased from Sigma Aldrich. The chemicals used for the synthesis of Schiff-base ligands and

[a]*Department of Chemical Sciences, Tezpur University, Napaam, Assam, India, 784028. E-mail: kusum@tezu.ernet.in*

[b]*Division of Crop Protection Chemicals, Indian Institute of Chemical Technology, Uppal Road, Hyderabad, Andhra Pradesh, India, 500607*

[c]*Center for NMR and Structural Chemistry, Indian Institute of Chemical Technology, Uppal Road, Hyderabad, Andhra Pradesh, India, 500607*

† Electronic supplementary information (ESI) available. See DOI: 10.1039/c5ra03492b

its corresponding Mn-complexes are manganese acetate, $Mn(OAc)_2 \cdot 4H_2O$ (Qualigens), salicylaldehyde and its derivatives (Alfa Aesar) and 1,1′-binaphthyl-2,2′-diamine (Sigma Aldrich). For the preparation of modified MCM-41 we used pyridine carboxaldehyde and 3-aminopropyl-triethoxysilane purchased from Sigma Aldrich. All the solvents are purified prior to use. Powder X-ray diffraction patterns of the samples are recorded on a Philips X'pert MPD diffractometer with Cu-Kα (λ = 1.5405 Å) radiation with a step size of 0.02° 2θ and a step time of 5 s and a curved Cu-Kα monochromator under identical conditions. The BET surface areas are determined with the use of N_2 sorption data measured at 77 K with a volumetric adsorption setup (NOVA 1000e, Quantachrome Instruments). The pore diameters of the samples are determined from the desorption branch of the N_2 adsorption isotherm with the Barret, Joyner, and Halenda (BJH) method. The electronic absorption spectra are recorded using a Hitachi U-3400 spectrophotometer with a diffuse reflectance attachment equipped with an integrating sphere of 60 mm inner diameter. Monochromatic light is used in the whole spectral region in order to minimize the effect of fluorescence. For recording the spectra of the MCM-41 immobilized metal complexes, the powdered samples are placed in a black absorbing hole (10 mm, in diameter and 3 mm deep) of a sample holder, and the surface is smoothed. The layer can be regarded as infinitely thick, as required by the Kubelka–Munk theory. The optical spectrums are then recorded in the reflectance mode. A Kubelka–Munk (KM) analysis[30] is performed on the reflectance data. The KM factor, $F(R)$, is given by $F(R) = (1 - R)^2/2R = k/s$ where R is the diffuse reflectance of the sample as compared to $BaSO_4$, k is the molar absorption coefficient, and s is the scattering coefficient of the sample. The infrared spectra in the range of 450–4000 cm^{-1} are recorded on a Perkin-Elmer Spectrum 2000 FTIR spectrometer. The spectra of the neat Mn-Schiff base complexes and the MCM-41 immobilized complexes are recorded as KBr pellets by mixing the samples well with KBr. The SEM and elemental chemical analyses are performed by using JEOL JSM-6390 LV at an acceleration voltage of 5–10 kV. The samples are deposited on a brass holder and sputtered with platinum. The cyclic voltammograms of neat and MCM-41 supported metal complexes are recorded using CHI-600A meter from CH Instruments, and 0.1 M TBAP (tetra-butyl ammonium phosphate) is used as the supporting electrolyte. For recording the cyclic voltammogram of the MCM-41 supported chiral Mn-Schiff base complex, the working electrode is prepared by taking a 1 : 1 weight ratio of metal complexes in 1 mL of DCM. This suspension is ultrasonicated for 15 min. 10 μL of this dispersion is coated on glassy carbon electrode and 5 μL of 5% styrene (as binder from Aldrich) is added on these coating and dried. The glassy carbon electrode is used as the working electrode and Ag/AgCl/KCl (saturated) is used as reference electrode. The cyclic voltammogram are recorded in water using TBAP as electrolyte. The cyclic voltammogram of neat complex is taken in solution mode, using 0.01 M of the metal complexes in a 0.1 M TBAP. MAS-NMR measurements are performed on Bruker ultrasheld 500 MHz WB NMR spectrometer at 11.75 T field producing ^{13}C and ^{29}Si Larmor frequencies at 125.77 and 130.31 MHz respectively. The samples are analyzed by placing in a 3.2 mm zirconia rotor by regulating the spinning speed at 10 kHz. The applied pulse width corresponding to an angle of $\pi/2$ for both the nuclei is 2.3 μs, with a recycle delay of 3 s. The chemical shift reference for ^{13}C spectrum is set at 77 MHz corresponding to $CDCl_3$ peak, and for ^{29}Si the reference is set at 0 ppm corresponding to the TSP single peak. The enantiomeric excess (ee) of the product was determined by HPLC (High Performance Liquid Chromatography) analysis using chiral columns (φ 4.6 mm × 250 mm, DAICEL CHIRALCEL OD-H or CHIRALPAK AD-H). CHNS/O-analyser, Perkin Elmer is used for elemental detection. Inductively Coupled Plasma (ICP) spectrometer analysis (Perkin Elmer, Model no. ICP Optima 2100 DV) and Atomic Absorption Spectroscopy (AAS, ICE 3500 Thermo Scientific) are used to detect %Mn in heterogeneous Mn(III)-Schiff base complexes.

2.2. Preparation of Schiff base ligands

In a 5 mL round-bottomed two-neck flask compound (*S*)-1,1′-binaphthyl-2,2′-diamine (200 mg, 0.704 mmol, 1 equiv.) dissolved in 4 mL of toluene and 2-hydroxybenzaldehyde was added (171 mg, 1.4 mmol, 2 equiv.). To this reaction mixture catalytic amount of *p*-toluenesulfonic acid (13 mg, 0.07 mmol, 0.1 equiv.) was added and the reaction mixture was stirred at 50–60 °C for 4 hours. The reaction mixture colour was changed to yellow; this reaction mixture was cooled to room temperature. Toluene was removed under reduced pressure. The crude residue was purified through a silica gel column using hexane and ethyl acetate as eluent (10/3) to give pure chiral (*S*) ligand-1, Scheme 1. The similar procedure was followed for the synthesis of ligands 2 and 3. The structures of the three ligands were

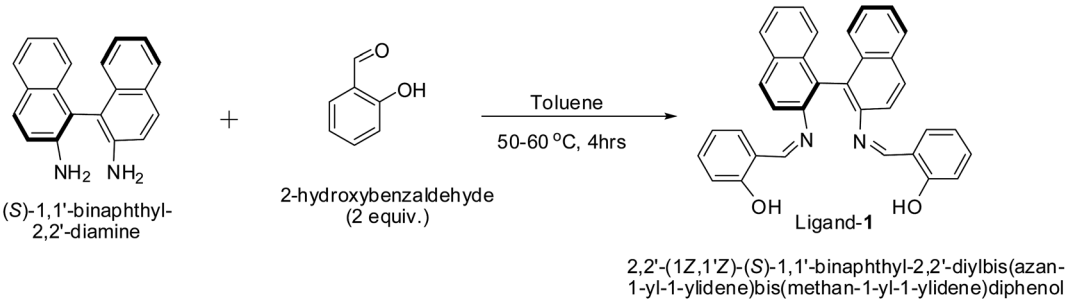

Scheme 1 Synthesis of Schiff base ligand.

confirmed from ^{1}H and ^{13}C NMR analysis. ^{1}H and ^{13}C NMR spectrums of the three ligands are provided in ESI.†

2.3. Preparation of Mn(III) Schiff base complexes (Mn-L1, Mn-L2 and Mn-L3)

To an ethanolic solution of (10 mL) $Mn(CH_3COO)_2 \cdot 4H_2O$ (10 mmol), a solution of either ligand L1/L2/L3 (5 mmol) was prepared in absolute ethanol (50 mL) under N_2 atmosphere and stirred under refluxed condition for 4–5 h. The resulting reaction mixture was then cooled to room temperature and solid LiCl (0.64 g, 15 mmol) was added to it and stirred for an additional 4 h while the reaction mixture was exposed to air and filtered. After complete evaporation of the solvent from the filtrate, the resulting residue was extracted with dichloromethane. The organic phase was washed with water and dried over Na_2SO_4. The drying agent was removed by filtration and the solution was concentrated to yield the desired complexes, Scheme 2.

2.4. Preparation of immobilized chiral metal complexes

The MCM-41 supported chiral manganese complexes were synthesized following the same procedure as we employed in our previous paper[31] shown in Scheme 3. In a typical procedure 2 g (~33.3 mmol) of MCM-41 and 0.3 g (1.67 mmol) of 3-aminopropyltrimethoxysilane and in 20 mL of toluene was refluxed at 80 °C with constant stirring for 24 h. After cooling to room temperature, the resultant white solid was collected after 1 h. The powder sample was then filtered and washed with diethyl ether and finally dried under vacuum for 12 h. To this amino functionalized MCM-41 (white solid product), 2 mmol of 4-pyridine carboxaldehyde was added and stirred at 75 °C for 16 h to obtain pyridine-carboxaldehyde-modified MCM-41. Solution of Mn-L1 or Mn-L2/Mn-L3 (1 mmol) prepared separately in ethanol (10 mL) was added to this-modified MCM-41 (1 g), and the resulting suspension was refluxed for 48 h. Resulting immobilized catalysts were filtered, washed thoroughly with dry toluene, and extracted repeatedly with methanol and dichloromethane on a Soxhlet extractor until the extraction liquid became colourless.

2.5. General procedure for oxidation of 2-naphthol

Oxidation of 2-naphthol to BINOL was carried out following the previous reported procedure.[12] In a typical catalytic process, 5 mmol of 2-naphthol along with 10 mL of methanol, 20 mg of catalyst were added into a 100 mL two-necked flask equipped with a condenser and an air pump. The reaction was started by passing the dry air with a stable flow rate of 80 mL min^{-1}

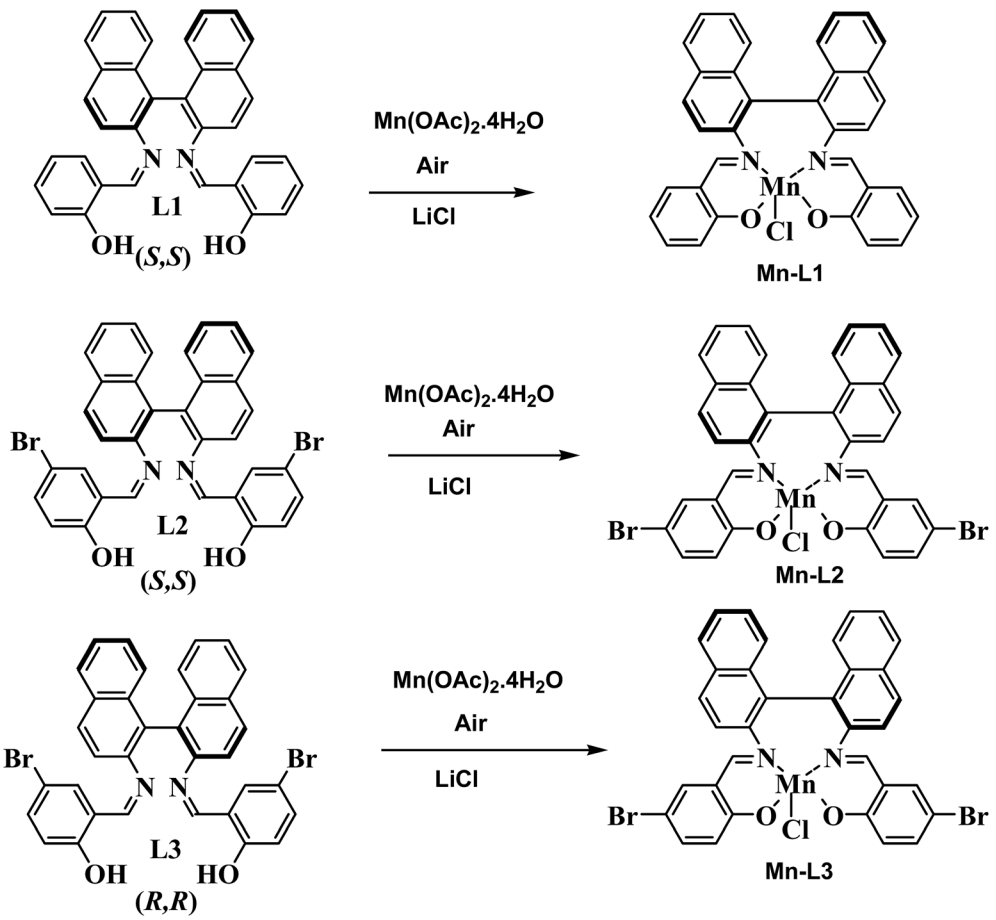

Scheme 2 Synthesis of Mn-Schiff base complexes.

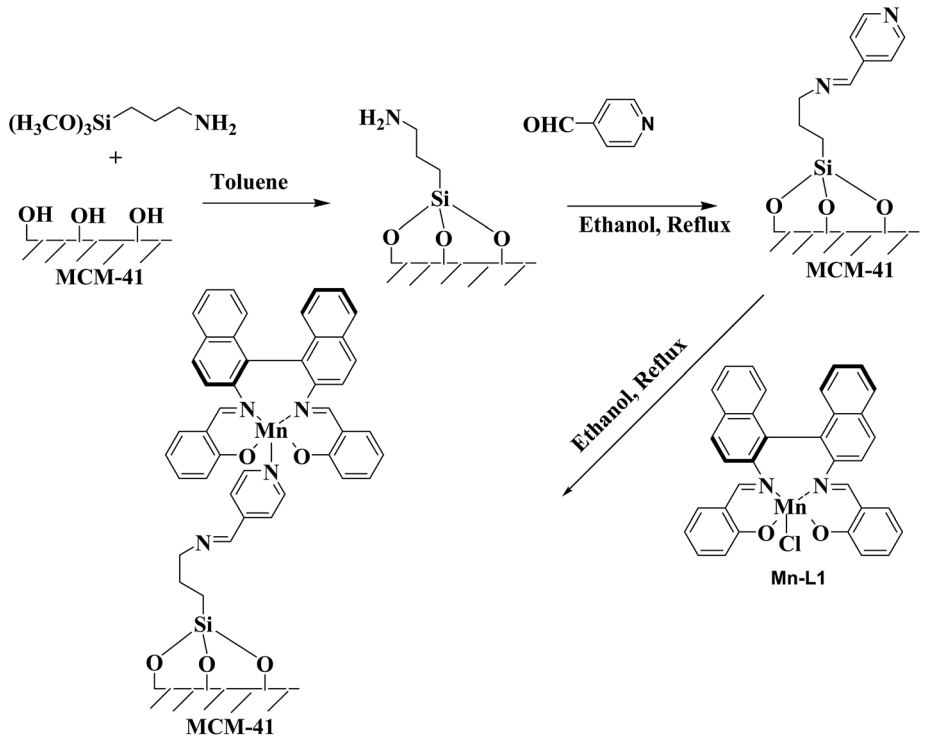

Scheme 3 Synthesis of MCM-41 supported Mn-Schiff base complexes.

controlled by a flow meter into the bottom of reactor at reaction temperature. The progress of the reaction was monitored by thin layer chromatography and after the completion of the reaction; the catalyst was filtered, washed with petroleum ether and dried at 100 °C overnight.

2.6. Rate dependence on 2-naphthol concentration

Kinetic study was performed by preparing a certain concentration of 2-naphthol (0.1 mmol to 1 mmol) in 2 mL toluene and warmed to 60 °C. The solution of the catalyst Mn-L1 (5.0 mg) in toluene (2 mL) and solid Mn-L1–MCM-41 (5.0 mg) catalyst was added at 60 °C in either case. The area ratios of 2-naphthol was analysed 5 times par 1 hour by HPLC to determine the consumption rate of 2-naphthol in the initial stage of the reaction. Similar kinetic measurements were also performed after 2nd and 3rd run of the Mn-L1–MCM-41 catalyst to understand recycled ability of the catalyst.

3. Results and discussion

In order to characterize the synthesized materials we have used various spectrochemical and physicochemical techniques like PXRD, FTIR, BET, UV-vis/DRS, cyclic voltammetry and SEM for their characterization. The details of which are described below separately. After confirming the formation of the desired materials we apply them as catalyst for catalytic oxidation of 2-naphthol to BINOL. The results of catalytic activity are presented after conferring the material characterization.

3.1. Powder X-ray diffraction study (PXRD)

X-ray diffraction pattern of neat MCM-41 and its modified counterparts are shown in Fig. 1. PXRD pattern of MCM-41 shows characteristic intense peak due to reflection at (100) plane and two low intense peak due to reflections at (110) and (200) planes.[32] Decrease in peak intensities and shifting in 2θ value is observed after modification with the linker and on immobilization of the metal complexes. The intensities of all peaks are found to decreases and intensities of 110 and 200 reflections decreases more on immobilization of metal complex over MCM-41, with little shifting in the 2θ value, Fig. 1c and d. Decrease in peak intensity and shifting of 2θ value towards lower value confirms the successful attachment of the chiral metal catalyst with modified MCM-41.

3.2. CHN analysis and surface area

Carbon (C), hydrogen (H) and nitrogen (N) contents in the three ligands, homogeneous and the heterogeneous complexes are determined by CHN analysis. Amount of metal content in homogeneous chiral complexes are estimated from UV-vis study while amounts of Mn-loading in the immobilized complexes are determined by inductively coupled plasma (ICP) spectrometer analysis. The amount of C, H and N along with the amount of Mn-content approximately matches with the expected formula (% calculated) of the metal complexes either in homogeneous or heterogeneous phase. The ratio of C/N is also found to match approximately with the expected ratio, Table 1. This further reveals that metal complexes are immobilized over the surface of MCM-41.

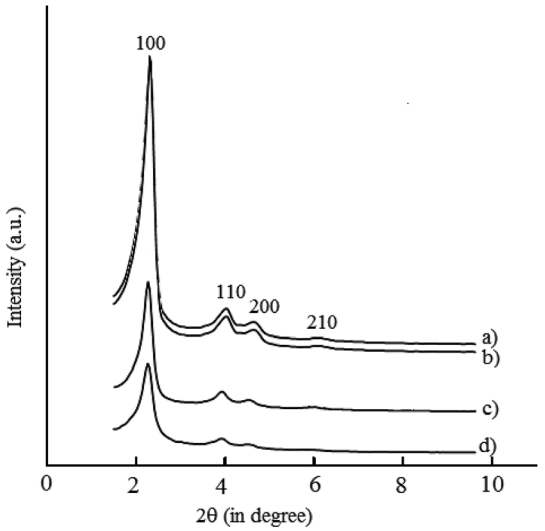

Fig. 1 XRD pattern of (a) MCM-41 (b) ammine functionalized MCM-41 (c) pyridine carboxaldehyde–MCM-41 (d) metal complexes immobilized in MCM-41.

MCM-41 and pyridine carboxaldehyde–MCM-41 shows typical type IV isotherm having three well-distinguished regions[33] mono and multilayer adsorption on the pore walls (region A), capillary condensation (region B), and multilayer adsorption on the outer surface (region C), Fig. 2a and b, respectively. The MCM-41 immobilized catalyst shows type III isotherm, indicating incorporation of metal complex into the pores of MCM-41 by a multi-step grafting method, Fig. 2c and d.[34] This is in agreement with the decrease of the pore volume of MCM-41 after incorporation of chiral Mn(III) Schiff base complexes. BET surface area, pore diameter, and pore volume are presented in Table 1. It is clearly observed that upon functionalization and immobilization BET surface area decreases significantly in comparison to MCM-41 precursor. The mesoporous diameter as well as the pore volume is also found to be less in case of the modified MCM-41. For example on immobilization of Mn-L2, the BET surface area get reduced from 1015 to 612 $m^2\ g^{-1}$, the pore size from 37 to 23 Å and pore volume from 0.576 to 0.448 $cm^3\ g^{-1}$.

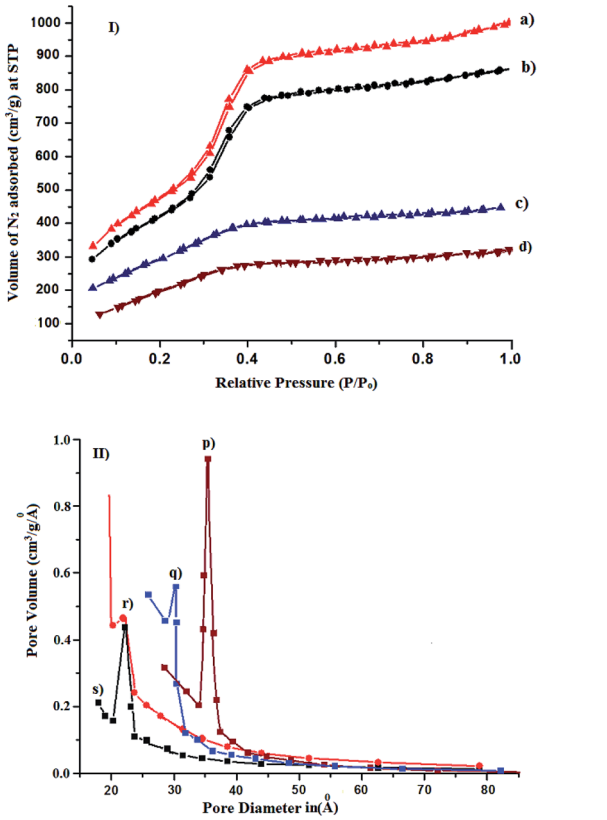

Fig. 2 N_2-adsorption isotherm of (I) (a) MCM-41 (b) pyridine carboxaldehyde–MCM-41 (c) Mn-L1–MCM-41 (d) Mn-L2–MCM-41. (II) Pore size distribution in (p) MCM-41 (q) pyridine carboxaldehyde–MCM-41 (r) Mn-L1–MCM-41 (s) Mn-L2–MCM-41.

3.3. FTIR and solid state ^{29}Si and ^{13}C NMR analysis

The FTIR spectrum of calcined MCM-41 is shown in Fig. 3a. The bands 1064 and 3464 cm^{-1} are characteristic for Si–O–Si and Si–OH bond, respectively.[32] In the FTIR spectra of amine functionalized MCM-41, four additional peaks are due to ν(N–H stretching), ν(C–H, stretching), ν(N–H bending) and ν(CH_2 bending), are observed at 3274, 2940, 1567 and 1492 respectively, (Fig. 3b). The functionalization of MCM-41 with amine *via* APTS is confirmed by the presence of N–H stretching and $-CH_2$ bending modes. After treating with pyridine

Table 1 BET and CHN analysis of MCM-41, PyC–MCM-41, Mn-L1–MCM-41, Mn-L2/Mn-L3–MCM-41. %Mn loading is calculated from ICP analysis. %Mn loading obtained from AAS and % calculated CHN analysis are shown in parenthesis

Compound	Mn-loading (mg/100 mg)	BJH pore diameter (Å)	Total pore volume ($cm^3\ g^{-1}$)	BET surface area ($m^2\ g^{-1}$)	Elemental analysis (%)		
					C	H	N
MCM-41	—	37	0.944	1015	—	—	—
PyC–MCM-41	—	30	0.576	745	10.62 (72.9)	2.13 (8.16)	2.32 (18.9)
L1	—	—	—	—	82.91	4.91	5.69
L2	—	—	—	—	62.79	3.41	4.31
Mn-L1	9.22 (9.24)	—	—	—	67.54 (70.54)	4.23 (4.23)	4.70 (4.70)
Mn-L2/Mn-L3	8.81 (8.82)	—	—	—	68.07 (65.77)	3.36 (3.08)	3.98 (3.72)
Mn-L1–MCM-41	7.75 (7.79)	22	0.465	618	71.46 (74.57)	5.27 (5.26)	6.46 (7.91)
Mn-L2/Mn-L3–MCM-41	6.35 (6.41)	23	0.448	612	61.34 (61.78)	4.54 (3.77)	5.55 (5.06)

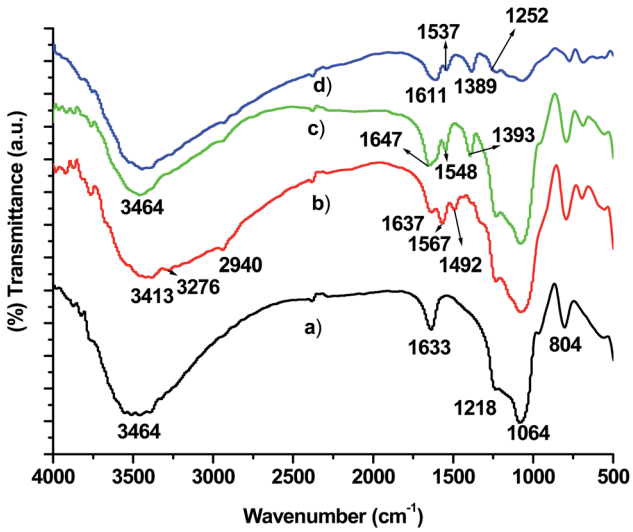

Fig. 3 FTIR spectrum of (a) MCM-41 (b) APTS–MCM-41 (c) pyridine carboxaldehyde–MCM-41 (d) typical FTIR spectrum of MCM-41 immobilized metal complexes.

carboxaldehyde, FTIR spectra shows peaks at 1647, 1548 and 1393 cm^{-1} corresponding to C=N, C=C (aromatic) and C–N stretching vibration. The absence of N–H vibrational band and presence of C=N bands further confirms the condensation of $–NH_2$ group of siloxyl moiety with –CHO group of pyridine carboxaldehyde and it do not possesses any peaks due to N–H vibrations. The functionalization of MCM-41 and its modification with pyridine carboxaldehyde are also confirmed by ^{29}Si and ^{13}C NMR analysis, details of which are already presented in our recently published work.[31]

After the confirmation of the formation of linker group on silica matrix, the chiral Mn-Schiff base complexes are anchored over MCM-41 *via* the formation of Mn–N bond with the linker group, Scheme 2. The FTIR spectrum of the MCM-41 immobilized complexes shows almost the similar bands with those of the neat complexes in the region of 1600–1200 cm^{-1}. The presence of most characteristics bands above 1600 cm^{-1} due to C=N confirms the immobilization of the metal complexes over MCM-41, Fig. 3d. The solid state ^{13}C NMR spectrum of the complexes also shows the characteristics peak corresponding to that of the co-ordinated ligand. The slight change in chemical shift ^{13}C NMR and ^{29}Si value in Fig. 4 is expected due to the change in the chemical environment upon immobilization over MCM-41.

3.4. UV-vis/DRS spectra

Typical UV-vis spectrum of ligand (L1), the neat Mn(III) metal complex, Mn-L1 and that of corresponding MCM-41 supported metal complex, Mn-L1–MCM-41 are shown in Fig. 5 as representative case. The nature of transition for particular wavelengths is depicted in Table 2. For instant ligand L1 gives absorption bands at 226, 275, 316 and 348 nm, Fig. 5a. Bands at 226 and 275 nm are due to $\pi \rightarrow \pi^*$ while those in the higher wavelengths corresponds to $n \rightarrow \pi$ transition. Mn-L1 complex shows absorption band at 208, 235, 285, 346 and 448 nm, Fig. 5b. The lower wavelength bands at 208 and 235 nm are due to $\pi \rightarrow \pi$ transition, bands at 285 and 346 nm results from charge transfer transition and that at 448 nm is because of d–d transition. Diffuse reflectance spectrum of the MCM-41 immobilized complexes, also shows bands approximately in the similar region, Fig. 5c and Table 2. The small change in the wavelengths can be attributed to the effect of the MCM-41 matrix. MCM-41 anchored Mn-L1 shows absorption bands resulting from $\pi \rightarrow \pi^*$, $d\pi \rightarrow p\pi$ and $d \rightarrow d$ transition. The most significant changes observed in case of Mn-L1 and Mn-L2/Mn-L3 when supported on MCM-41 is the appearance of band above 600 nm. The band above 600 nm can be attributed to transition from a $d\pi$ orbital (HOMO) to a $p\pi$-orbital of ligand (LUMO) mostly concentrated on pyridine linkage.

3.5. Cyclic voltammetry study

The electrochemical behaviour of the ligands and the neat and the MCM-41 supported metal complexes are studied by means cyclic voltammetry. The cyclic voltammogram of the two ligands L1 and L2/L3 are shown in Fig. 6. Both the ligands L1 and L2/L3, respectively shows one irreversible reduction peak at 0.236 V and 0.239 V *versus* Ag/AgCl. In addition to this Br-substituted ligand L2/L3 shows an additional peak at −0.511 V due to reduction of –Br. This behaviour was observed for a wide range of scan rates from 0.005 to 0.1 V s^{-1}. Hence, such a reduction process should correspond to a totally irreversible electron transfer. For all Schiff bases under study, this irreversible reduction peak would be ascribed to an intramolecular reductive coupling of the two imine groups to yield a piperazine.[35] Such a process would involve self-protonation reactions where the phenolic hydroxyl groups act as proton donors. E_{pc} becomes less negative according to the sequence H < Br, *i.e.* in order of an increase in both electron-withdrawing and π-acceptor qualities of the substituents.

All the three Mn-Schiff base complexes exhibits a redox couple (Mn^{III}/Mn^{II}) in the range of −0.4 to 0.4 V. Redox potentials values for the corresponding complexes are given in a Table 3 and a typical cyclic voltammogram of Mn-L1 is shown as a representative case in Fig. 7a. The presence of quasi reversible one electron oxidation–reduction wave gives an additional proof that compounds are of Mn(III). The slight difference in the redox potential values of Mn-L1 with those of Mn-L2 or Mn-L3 is due to the substituent effect on the phenyl ring. Moreover, for all complexes studied, the cathodic wave corresponding to the irreversible reduction of the ligand moiety is no longer observed. This indicates that due to lack of transferable hydroxylic protons, the reduction potentials of the ligands get shifted to lower limit in comparison to the potential interval considered in the experimental measurements. The cyclic voltammogram of the corresponding MCM-41 supported complexes also shows a quasi reversible redox couple which is differed from those of the neat complexes. A representative voltammogram of which is shown in figure, Fig. 7c. Potential values for the immobilized complexes were found to be differed from the parent complexes due to different co-ordination

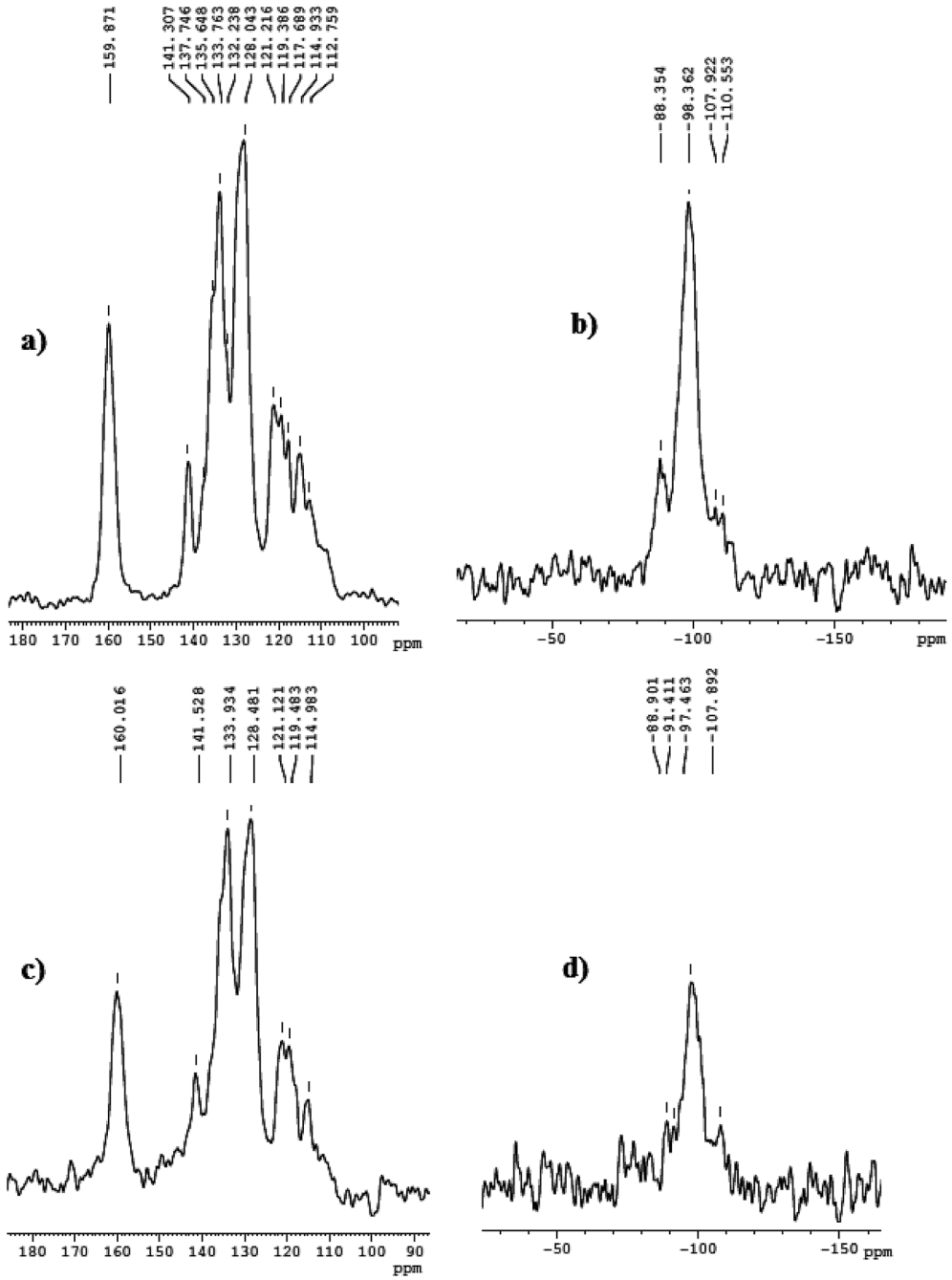

Fig. 4 (a) and (b) are ^{13}C and ^{29}Si NMR spectra for Mn-L1–MCM-41 while (c) and (d) are those for Mn-L2–MCM-41.

environment as well as due to matrix effect or confinement effect.[20]

Cyclic voltammograms of the metal complexes were also recorded in different scan rate ranging from 0.005 V to 0.1 V, Fig. 7b and d. Lowering of the scan results in decrease in peak current and a linear plot of square root of scan rate *vs.* peak (Fig. 8a) indicates the electron transport occurs through a normal diffusion controlled process in solution. Similar to the neat complexes, in case of the MCM-41 supported complexes peak current is found to finish on lowering the scan rate. Linear plot of scan rate *vs.* peak current further signifies for surface controlled process, Fig. 8b.

3.6. SEM-analysis

Scanning electron microscopic images of MCM-41 and MCM-41 immobilized Mn(III)-Schiff base complexes are taken in different magnification (×3000 to ×10 000) are shown in Fig. 9. From the SEM images it is observed that immobilization of metal complexes through the above mentioned processes has not lead to any change in morphology of MCM-41. Presence of agglomerate particle clearly observed from highly magnified SEM images can be attributed to the formation of metal of complexes on surface of MCM-41. Similar observations were also made in our previous work[31] as well as in various other

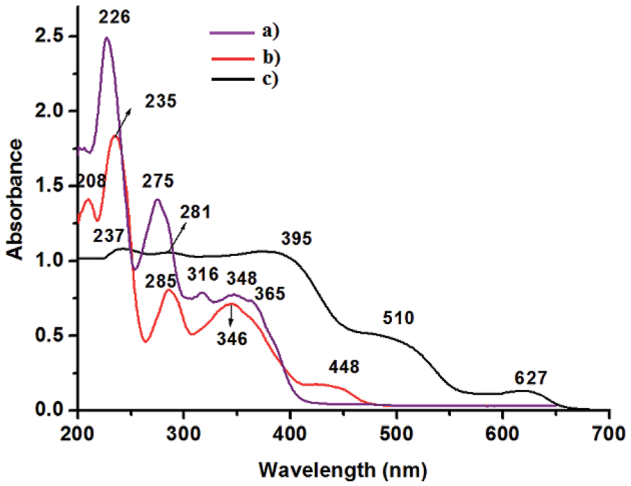

Fig. 5 (a) and (b) represents the typical UV-vis spectra of ligands and Mn(III) complexes, respectively. (c) Corresponding UV-vis/DRS of the MCM-41 supported metal complexes.

reports.[28,29] Thus the presence of agglomerate particle confirms the successful immobilization of Mn-Schiff base complexes over MCM-41.

4. Catalytic activity

The three catalysts were screened for the oxidation of 2-naphthol performed under aerobic conditions and at different catalytic condition. In a preliminary experiment, the reaction of 2-naphthol (5 mmol) with Mn-L1 (10 mg) catalyst was performed in toluene at ambient temperature in absence of air. Reaction did not proceed at all upto 4 days indicating that catalyst alone can not oxidize 2-naphthol. Introduction of air into the reaction mixture at 10 mL min^{-1}, leads to slow conversion of 2-naphthol to BINOL. Enhancement of air flow up to 80 mL min^{-1} led to almost 62% conversion of 2-naphthol with Mn-L1 complex. Conversely, the rate of air flow was also found to affect the %yield and enantioselectivity (%ee) of the product. For instant in presence of Mn-L1 catalyst (10 mg) when the rate of air flow was 10 mL min^{-1} the %yield and the %ee (*S*-BINOL) was found to be 3% and 9%, respectively whereas with rate flow of 80 mL min^{-1} 57% yield and 67% ee, was obtained, Table 4. Further increase in air flow did not lead to any increase in conversion rate. While performing the reaction with MCM-41 in presence of air no conversion of 2-naphthol was observed upto several days indicating that metal source is essential for the catalytic conversion. MCM-41 supported metal complex Mn-L1–MCM-41 under identical condition however; result in 65% conversion with 62% yield and 69% ee. The slight higher catalytic activity observed in case of the heterogeneous catalyst can be attributed to the difference in active site availability under homogeneous and heterogeneous catalyst.

Temperature, nature of solvent and catalyst amount plays an important role in catalytic oxidation processes.[31] Effect of temperature, solvent polarity and amount of catalyst was monitored by considering Mn-L1 and Mn-L1–MCM-41 as test catalysts. To observe the effect of temperature, we considered a wide range of temperature *viz* room temperature (rt, 32 °C) to −30 °C and performed the reaction using toluene as solvent. Results obtained from such observation are depicted in Table 5. In presence of Mn-L1 complex maximum yield (90%) and ee (83%) was obtained at −10 °C. However, further decrease in temperature resulted in decrease of enantioselectivity. At −30 °C both the yield and ee was found to decrease dramatically. On increasing the temperature from 32 to 100 °C, no significant enhancement in catalytic activity was observed. So we considered, −10 °C as the optimize

Table 2 Assignment of UV-vis/DRS transitions in synthesized complexes

Compound	Wavelength	Transition
Ligand 1, L1	226, 275	$\pi \rightarrow \pi^*$
	316, 348, 365	$n \rightarrow \pi^*$
Ligand 2 (L2) or ligand 3 (L3)	235, 278	$\pi \rightarrow \pi^*$
	312, 348, 372	$n \rightarrow \pi^*$
Mn-L1	208, 235	$\pi \rightarrow \pi^*$
	285, 346	$d\pi \rightarrow p\pi^*$
	448	$d \rightarrow d$
Mn-L2 or Mn-L3	212, 236	$\pi \rightarrow \pi^*$
	265, 388	$d\pi \rightarrow p\pi^*$
	461	$d \rightarrow d$
Mn-L1–MCM-41	237, 281	$\pi \rightarrow \pi^*$
	395	$d\pi \rightarrow p\pi^*$
	510	$d \rightarrow d$
	627	$d\pi \rightarrow p\pi^*$(pyridine carboxaldehyde)
Mn-L2/L3–MCM-41	239, 277	$\pi \rightarrow \pi^*$
	386	$d\pi \rightarrow p\pi^*$
	505	$d \rightarrow d$
	617	$d\pi \rightarrow p\pi^*$(pyridine carboxaldehyde)

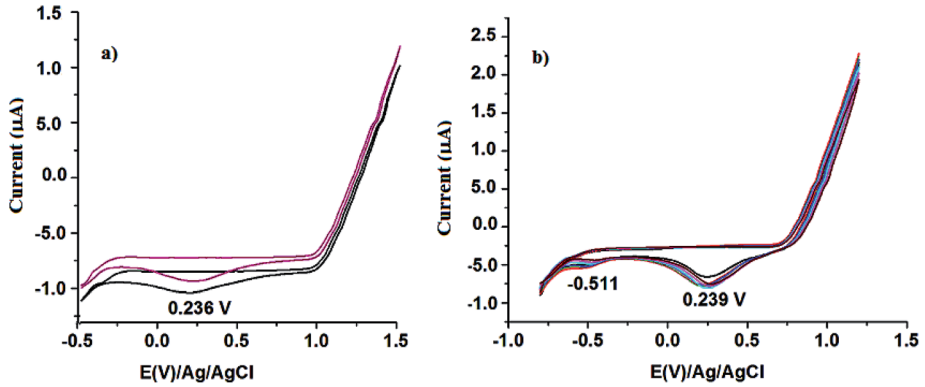

Fig. 6 Cyclic voltammogram of ligand 1 and ligand 2/ligand 3.

Table 3 Redox potential values of the ligand and metal complexes

Compound	E^{ox}	E^{red}
Ligand 1, L1	—	0.236
Ligand 2 (L2) or ligand 3 (L3)	—	0.239
Mn-L1	−0.030	−0.178
Mn-L2 or Mn-L3	−0.034	−0.184
Mn-L1–MCM-41	−0.166	−0.271
Mn-L2/L3–MCM-41	−0.169	−0.281

temperature for the catalytic reaction. It is pertinent to mention herein that effect of temperature do not readily follows the Arrhenius law. The anomalous change in %ee with respect to temperature can be explained by considering following two eqn (1) and (2). As per the eqn (1), relative rate constant (ln K) for the formation of (S)- and (R) BINOL in the oxidation of 2-naphthol can be correlated with ee's of the reaction and can be written in the form of differential Eyring equation as shown in eqn (2).[36]

$$\ln\left[\frac{K_s}{K_R}\right] = \ln\left[\frac{(100 + \%ee)}{(100 - \%ee)}\right] \quad (1)$$

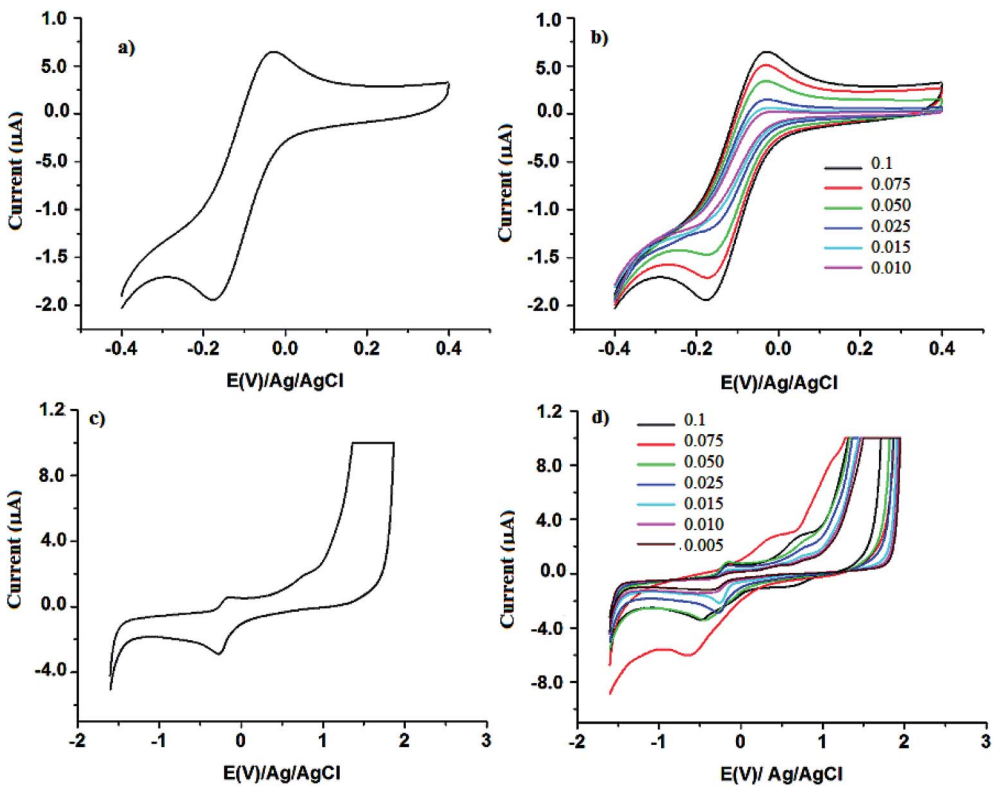

Fig. 7 Cyclic voltammogram of (a) Mn-L1 (b) that of in different scan rate (0.010 V to 0.1 V) (c) CV of Mn-L1–MCM-41 and (d) that of in different scan rate (0.005 V to 0.1 V).

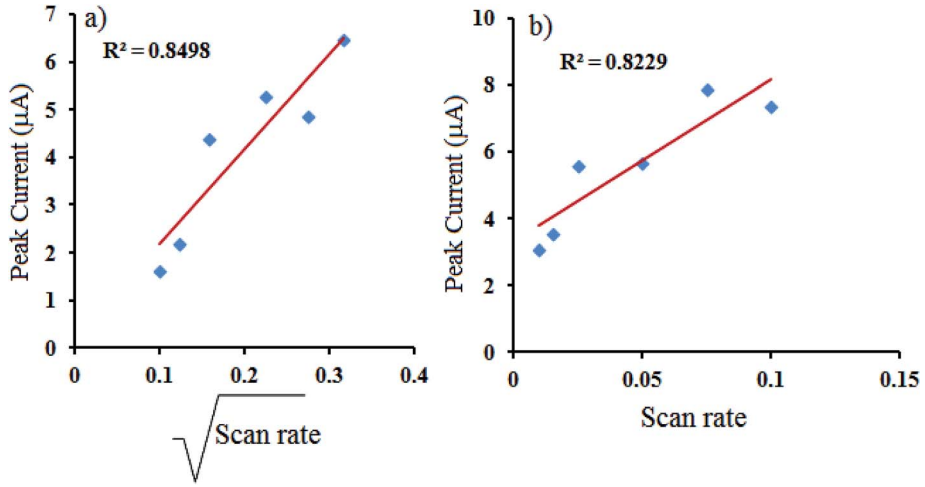

Fig. 8 (a) Plot of square root of scan rate *vs.* peak current (for Mn-L1 complex), (b) plot of scan rate *vs.* peak current (for Mn-L1–MCM-41).

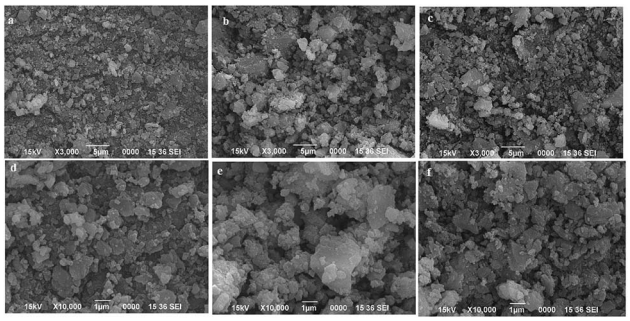

Fig. 9 SEM image of (a) MCM-41 (b) Mn-L1–MCM-41 (c) Mn-L2–MCM-41. (d)–(f) are SEM images of the same respectively in high magnification.

$$\ln\left[\frac{K_s}{K_R}\right] = \frac{-\Delta\Delta H^{\ddagger}}{RT} + \frac{\Delta\Delta S^{\ddagger}}{R} \quad (2)$$

If the mechanism of enantioselection remain constant over a wide range of temperature variation then according to eqn (2), a linear plot ($\ln(K_s/K_R)$ *vs.* $1/T$) would be expected provided $\Delta\Delta H^{\ddagger}$ and $\Delta\Delta S^{\ddagger}$ remains constant under that situation. On the other hand, if the enantio determining step is changing at different temperatures, a non-linear curve is expected as $\Delta\Delta H^{\ddagger}$ and $\Delta\Delta S^{\ddagger}$ values will no longer remains constant. In the present case the plot of $\ln(K_s/K_R)$ *vs.* $1/T$ shown in Fig. 10 is found to be nonlinear. Therefore it can be considered that the enantio determining step is changing over the range of temperatures examined in the current state of art. Thus, the observed reversal in absolute induction could arise from a temperature-dependent interchange of the enantio determining mechanisms. In case of the heterogeneous complex, Mn-L1–MCM-41, we observed (Table 5) almost similar trend in catalytic activity with respect to change in temperature *i.e.* the sense of induction is reversed in accordance with Arrhenius law and also improved with decreasing temperature from room temperature to −10 °C. In general Arrhenius law holds well only if the process follows the same reaction sequence. Once the temperature is increased the rate of the reaction will increase but at the same time supply of molecules to the surface may become slow and in that case Arrhenius plot will change slope. In the present case reverse temperature effect is possible since adsorption and surface concentration is a function of temperature especially when the

Table 4 Oxidation of 2-naphthol using Mn-L1 and Mn-L1–MCM-41 as catalyst[a] in different rate of O_2 flow

	Conversion[b] (%)		Yield[c] (%)		*R* : *S* (%)		%ee[d] (*S*)	
Air flow mL min^{-1}	Mn-L1	Mn-L1–MCM-41	Mn-L1	Mn-L1–MCM-41	Mn-L1	Mn-L1–MCM-41	Mn-L1	Mn-L1–MCM-41
10	5	7	3	5	35 : 65	32 : 68	9	11
20	12	15	9	12	31 : 69	31 : 69	12	12
30	23	27	18	21	33 : 67	34 : 66	16	18
40	32	38	27	34	34 : 66	29 : 71	21	23
50	38	41	30	37	32 : 68	26 : 74	44	49
60	47	52	38	47	27 : 73	27 : 73	57	59
70	57	59	48	51	25 : 75	26 : 74	62	63
80	62	65	57	62	22 : 78	20 : 80	67	69

[a] Reaction conditions: catalyst 10 mg, 2-naphthol 5 mmol, solvent 10 mL at 32 °C. [b] Determined by GC, conversion (%) = [moles of reactant converted] × 100]/[moles of reactant in feed]. [c] Isolated yield. [d] Determined by chiral HPLC analysis.

Table 5 Oxidation of 2-naphthol using Mn-L1 and Mn-L1–MCM-41 as catalyst and O_2 as oxidant (80 mL min^{-1}) in different temperature[a]

	Conversion[b] (%)		Yield[c] (%)		$R:S$ (%)		%ee[d] (S)	
Temp[r] (°C)	Mn-L1	Mn-L1–MCM-41	Mn-L1	Mn-L1–MCM-41	Mn-L1	Mn-L1–MCM-41	Mn-L1	Mn-L1–MCM-41
32	62	65	57	62	22 : 78	20 : 80	67	69
15	64	67	59	64	35 : 65	33 : 67	68	72
10	65	66	60	64	32 : 68	28 : 72	73	76
5	65	66	60	65	27 : 73	25 : 75	74	76
0	70	72	64	67	23 : 77	24 : 76	78	81
−5	70	72	64	67	26 : 74	24 : 76	78	82
−10	90	94	78	86	63 : 37	30 : 70	83	85
−15	82	86	72	81	34 : 66	26 : 74	80	84
−20	74	82	68	76	20 : 80	18 : 82	74	78
−25	70	75	63	69	27 : 73	22 : 78	71	73
−30	65	68	54	61	28 : 72	24 : 76	65	69

[a] Reaction conditions: catalyst 10 mg, 2-naphthol 5 mmol, solvent 10 mL. [b] Determined by GC, conversion (%) = [moles of reactant converted] × 100]/[moles of reactant in feed]. [c] Isolated yield. [d] Determined by chiral HPLC analysis.

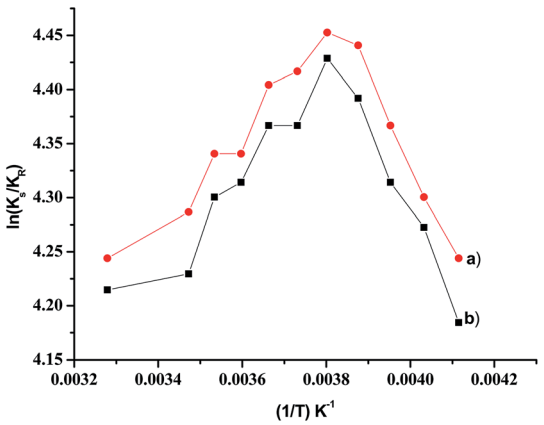

Fig. 10 Plot of $\ln(K_s/K_R)$ *vs.* $1/T$ (a) for reaction catalyzed by Mn-L1 complex and (b) for reaction catalyzed by Mn-L1–MCM-41.

molecule has to adsorb in particular mode to give stereospecificity or other preferred products. Further, lowering of the temperature from 32 °C to −10 °C, the partition coefficient (K) values were found to increase from 2.96 to 3.68. However, further decrease in temperature decreases the partition coefficient value. Thus the reaction was performed at −10 °C within a pH range 6.5 to 6.8.

To observe the effect of solvent, we choose both polar and non-polar solvents of different dielectric constant as listed in Table 6. In presence of both homogeneous and heterogeneous chiral Mn-L1 catalyst, conversion of 2-naphthol to BINOL was found to proceed well in non-polar solvents. Reaction does not at all proceed in water as solvent and apart from toluene the reaction proceed well in CCl_4 with maximum yield upto (80%) and enantioselectivity (72%). Thus, considering toluene as suitable solvent for the oxidation process, we performed all the reaction in toluene using the other homogeneous and heterogeneous catalyst. Same reaction was also performed by varying the amount of Mn-L1 and Mn-L1–MCM-41 catalyst from 5 mg to 25 mg keeping the amount of the substrate constant. Maximum yield above 88% and ee upto 91%, *S*-BINOL was obtained with 20 mg of the catalyst, Table 7. No significant enhancement in the catalytic process was observed on further increment of the catalytic amount. Thus we found the optimum condition for the reaction as temperature, −10 °C, solvent, toluene and catalytic amount to be 20 mg.

The reaction is then performed using the other homogeneous and MCM-41 supported chiral Mn(III) complexes under the above optimized condition. The % of conversion and selectivity ($R:S$ ratio) of the reactions are given in Table 7. Comparison of the catalytic activity of the homogeneous and heterogeneous systems indicates that chiral Mn-complexes immobilized in MCM-41 gives slightly better yield and ee. This enhancement in catalytic activity on immobilization into MCM-41 can be attributed to the chiral enhancement due to the confinement effect associated with such macroporous systems. It is also reported that by anchoring or immobilizing the catalysts onto micro porous and mesoporous materials, there is a significant increase in ee as compared to its homogenous analogue.[29,32]

To examine the role of the Schiff base in reaction, the reaction is performed in presence of MCM-41 and the two Schiff base ligands. We first performed the reaction using of 20 mg of MCM-41 and 5 mmol of Schiff base complex at −10 °C in toluene. MCM-41 in presence of chiral ligands does not lead to any coupling product. This shows that the metal complex is required to bring out the enantioselective coupling of 2-naphthol.

Several mechanisms *viz.* radical–radical and radical–anion couplings, have been proposed for oxidative coupling of 2-naphthol to BINOL. The radical–anion coupling is considered to be the most plausible mechanism for such cross-coupling reaction.[37,38] It has been reported that radical–anion coupling can be either a first or second-order dependence of the rate on substrate concentration.[15] In order to understand the proper reaction conditions for the cross-coupling reaction, we study the kinetics of this Mn-Schiff base complexes mediated aerobic oxidative coupling using Mn-L1 and Mn-L1–MCM-41 as the catalyst. A linear plot is obtained on plotting the amount of 2-

Table 6 Oxidation of 2-naphthol using Mn-L1 and Mn-L1–MCM-41 as catalyst and O_2 as oxidant in different solvents[a]

	Conversion[b] (%)		Yield[c] (%)		$R:S$ (%)		%ee[d] (S)	
Solvent	Mn-L1	Mn-L1–MCM-41	Mn-L1	Mn-L1–MCM-41	Mn-L1	Mn-L1–MCM-41	Mn-L1	Mn-L1–MCM-41
CH_3OH	16.5	17.2	9.2	10	38 : 62	31 : 69	15	15
C_2H_5OH	13.2	15.4	8.9	12.3	39 : 61	28 : 72	18	21
H_2O	Nil	—	—	—	—	—	—	—
CH_3CN	16.2	18.4	10.6	15.2	33 : 67	24 : 66	25	29
DMF	21.5	23.2	16.8	19.5	36 : 64	44 : 56	22	21
CH_2Cl_2	30.2	30.8	24.2	26.2	63 : 37	30 : 70	27	30
$CHCl_3$	44.3	47.6	26.5	30.5	34 : 66	26 : 74	39	44
Hexane	56	66	30	60	17 : 83	12 : 88	64	62
CCl_4	87	88	75	80	13 : 87	11 : 89	72	67

[a] Reaction conditions: catalyst 10 mg, 2-naphthol 5 mmol, solvent 10 mL, temperature −10 °C. [b] Determined by GC, conversion (%) = [moles of reactant converted] × 100]/[moles of reactant in feed]. [c] Isolated yield. [d] Determined by chiral HPLC analysis.

Table 7 Oxidation of 2-naphthol using 20 mg of different catalysts and air as oxidant in toluene at −10 °C

Catalyst	Time (h)	Conv.[a] (%)	Yield[b] (%)	$R:S$	%ee[c]
Oxidant (air)	26	—	—	—	
$Mn(OAc)_2 \cdot 4H_2O$	36	—	—	—	—
$Mn(OAc)_2$ + air	24	30	15	50 : 50	—
Mn-L1	36	—	—	—	—
Mn-L2	36	—	—	—	—
Mn-L3	36	—	—	—	—
Mn-L1 + air	42	83	79	16 : 84	82(S)
Mn-L2 + air	42	86	82	82 : 18	78(R)
Mn-L3 + air	42	85	82	7 : 93	83(S)
Mn-L1–MCM-41 + air	27	94	88	19 : 81	91(S)
Mn-L2–MCM-41 + air	34	89	87	95 : 5	87(R)
Mn-L3–MCM-41 + air	34	88	87	8 : 92	85(S)

[a] Determined by GC, conversion (%) = [moles of reactant converted] × 100]/[moles of reactant in feed]. [b] Isolated yield. [c] Determined by chiral HPLC analysis.

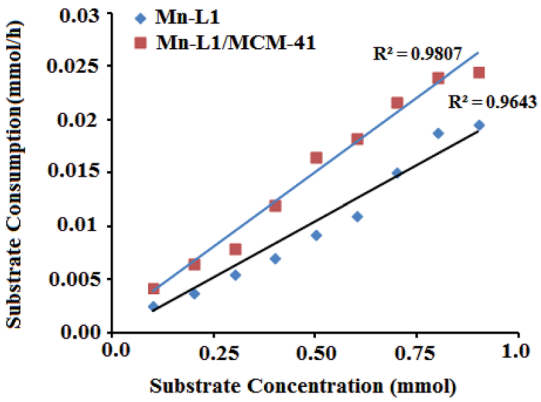

Fig. 11 Dependence of the rate on substrate concentration for the reaction catalysed by Mn-L1 and Mn-L1–MCM-41.

naphthol consumed (mmol h^{-1}) against the concentration of the substrate, Fig. 11. This suggests that the reaction follows a first order kinetics in presence of both the homogeneous and heterogeneous chiral Mn-L1 catalyst.

5. Recyclability test

The homogeneous chiral Mn(III) could not be retrieve whereas we could successfully recover the MCM-41 supported chiral catalyst. Recyclability test were performed under similar conditions using the immobilized catalyst Mn-L1–MCM-41 and Mn-L2–MCM-41. The catalysts were separated by centrifugation after first run and fresh reactants were added to the supernatant for the second cycle. Analysis of the reaction mixture shows no further change in the conversion of 2-naphthol to BINOL. No trace amount of metal complex was obtained in the UV-vis study of the supernatant. After separation, catalyst were washed thoroughly with dichloromethane (toluene), dried, and subjected to another cycle with fresh reactants under similar conditions. The conversion, %yield and %ee were found to be consistent. The above procedure is repeated for three cycles, and we do not observe any substantial loss in the catalytic activity of the immobilized catalyst. This indicates that the chiral Mn(III) salen complex is strongly bonded to the nitrogen atom of pyridine carboxaldehyde modified MCM-41 through the axial coordination. Kinetic study after 2nd and 3rd cycle also suggest for first order reaction and the amount of 2-naphthol consumed in both the cycles was found to be almost consistent with respect to the first cycle. However, after third cycle *i.e.* in fourth and fifth cycle we observed substantial decrease in the catalytic activity. Results of the %conversion, %yield and %ee obtained after 2nd, 3rd, 4th and 5th run are provided in ESI Table S1.† In order to understand the reason behind the loss in catalytic activity after third cycle, we performed ^{13}C NMR analysis and cyclic voltammetry study on the recovered catalyst Mn-L1–MCM-41, Fig. 12. ^{13}C NMR confirms that the complexes get ruptured after third cycle. Cyclic voltammetry patterns as well as the redox potential values were also found to be completely different from the original complex. Thus the change in redox potential values as well structural modification after completion of third cycle clearly supports the loss of catalytic activity. %Mn loading as obtained from ICP and AAS analysis (Table S2†) was also found to be less after 3rd cycle in comparison initial catalysts suggesting a substantial metal leaching. Thus, because of the change in redox potential values,

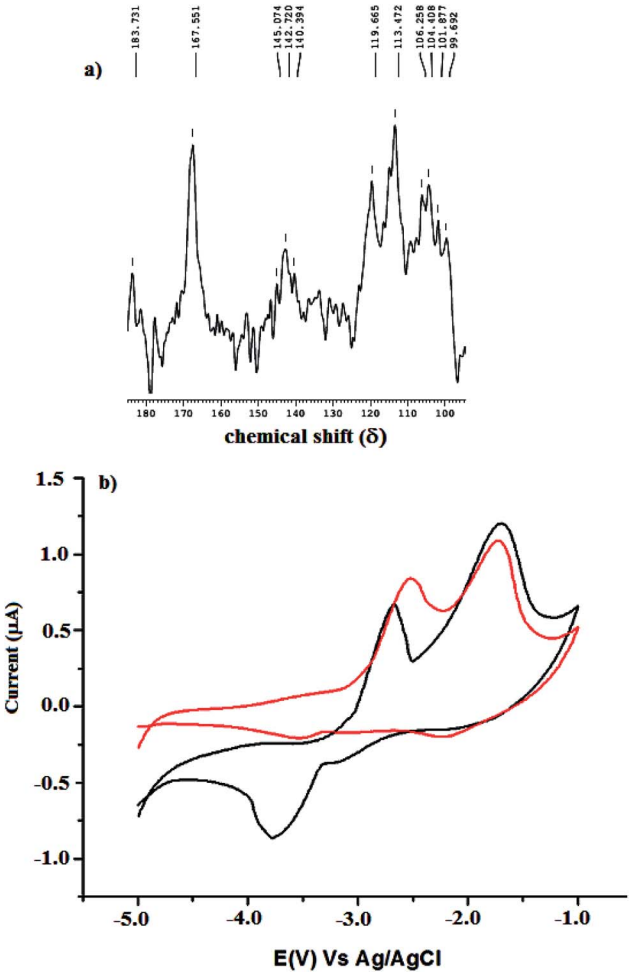

Fig. 12 (a) ^{13}C NMR spectra of Mn-L1–MCM-41 (b) cyclic voltammogram of Mn-L1–MCM-41 after fourth and fifth cycle.

structural deformation and sufficient metal leaching results in the deactivation of the catalysts after performing for three consecutive cycles.

6. Conclusion

In conclusion it can be said that three MCM-41 supported chiral Mn(III)-Schiff base complex are synthesized and characterized *via* various spectrochemical and physicochemical techniques. Three chiral complexes were found to be effective catalyst for oxidation of 2-naphthol to *C*2-symmetric (*R*)/(*S*)-BINOL. Catalytic activities of the three complexes were found to depend on various physical parameters such as nature of solvent, temperature and catalytic amount. Highest yield and enantioselectivity were achieved at −10 °C and in toluene with 20 mg of the catalyst. Heterogeneous catalysts were found to be equally active as the homogenous one and they could be recycled for three consecutive cycles without any loss of catalytic activity. Comparison of the catalytic activity of these catalysts with those of the other reported catalysts are found to be almost comparable.[14–18] Thus the present work could provide a new additional input in designing of newer heterogeneous chiral catalyst for asymmetric oxidative coupling of 2-naphthol.

References

1 J.-Q. Yu and Z. Shi, *C–H Activation, Topics in Current Chemistry*, Springer-Verlag, Berlin, 2010, vol. 292.
2 R. H. Crabtree, *J. Chem. Soc., Dalton Trans.*, 2001, 2437–2450.
3 A. E. Shilov and G. B. Shul'pin, *Chem. Rev.*, 1997, **97**, 2879–2932.
4 G. Chelucci and R. P. Thummel, *Chem. Rev.*, 2002, **102**, 3129–3170.
5 E. I. Solomon, U. M. Sundaram and T. E. Machonkin, *Chem. Rev.*, 1996, **96**, 2563–2606.
6 *Comprehensive Asymmetric Catalysis*, ed. E. N. Jacobsen, A. Pfaltz and H. Yamamoto, Springer-Verlag, Berlin, Heidelberg, 1999.
7 J. M. Brunel, *Chem. Rev.*, 2005, **105**, 857–897.
8 R. Noyori, *Asymmetric Catalysis in the Organic Synthesis*, Wiley, New York, 1994.
9 R. S. Coleman and M. L. Madaras, in *The Chemical Synthesis of Natural Products*, ed. K. J. Hale, CRC Press, Sheffield, 2000, ch. 6, pp. 144–179.
10 V. B. Sharma, S. L. Jain and B. Sain, *Tetrahedron Lett.*, 2003, **44**, 2655–2656.
11 D. R. Hwang, C. P. Chen and B. J. Uang, *Chem. Commun.*, 1999, 1207–1208.
12 E. Armengol, A. Corma, H. García and J. Primo, *Eur. J. Org. Chem.*, 1999, **1999**, 1915–1920.
13 M. Matsushita, K. Kamata, K. Yamaguchi and N. Mizuno, *J. Am. Chem. Soc.*, 2005, **127**, 6632–6640.
14 H. Egami and T. Katsuki, *J. Am. Chem. Soc.*, 2009, **131**, 6082–6083.
15 H. Egami, K. Matsumoto, T. Oguma, T. Kunisu and T. Katsuki, *J. Am. Chem. Soc.*, 2010, **132**, 13633–13635.
16 R. Irie, K. Masutani and T. Katsuki, *Synlett*, 2000, **2000**, 1433–1436.
17 C. Y. Chu, D. R. Hwang, S. K. Wang and B. J. Uang, *Chem. Commun.*, 2001, 980–981.
18 S. W. Hon, C. H. Li, J. H. Kuo, N. B. Barhate, Y. H. Liu, Y. Wang and C. T. Chen, *Org. Lett.*, 2001, **3**, 869–872.
19 D. J. Cole-Hamilton, *Science*, 2003, **299**, 1702–1706.
20 K. K. Bania, G. V. Karunakar, B. Sarma and R. C. Deka, *ChemPlusChem*, 2014, **79**, 427–438.
21 D. J. Xuereb and R. Raja, *Catal. Sci. Technol.*, 2011, **1**, 517–534.
22 J. M. Thomas and R. Raja, *Acc. Chem. Res.*, 2008, **41**, 708–720.
23 S. K. Das, S. P. Mahanta and K. K. Bania, *RSC Adv.*, 2014, **4**, 51496–51509.
24 M. Tada, N. Kojima, Y. Izumi, T. Taniike and Y. Iwasawa, *J. Phys. Chem. B*, 2005, **109**, 9905–9916.
25 M. Tada, T. Taniike, L. M. Kantam and Y. Iwasawa, *Chem. Commun.*, 2004, 2542–2543.
26 K. K. Bania, D. Bharali, B. Viswanathan and R. C. Deka, *Inorg. Chem.*, 2012, **51**, 1657–1674.
27 M. E. Davis, *Nature*, 2002, **417**, 813–821.

28 P. Piaggio, D. McMorn, P. Murphy, D. Bethell, P. C. Bullman-Page, F. E. Hancock, C. Sly, O. J. Kerton and G. J. Hutchings, *J. Chem. Soc., Perkin Trans. 2*, 2000, 2008–2015.
29 R. I. Kureshy, I. Ahmad, N. H. Khan, S. H. R. Abdi, K. Pathak and R. V. Jasra, *J. Catal.*, 2006, **238**, 134–141.
30 H. G. Hecht, in *Modern Aspect of Reflectance Spectroscopy*, ed. W. W. Wendlandt, Plenum Press, New York, 1968.
31 M. Mandal, V. Nagaraju, B. Sarma, G. V. Karunakar and K. K. Bania, *ChemPlusChem*, 2015, **80**, 749–761.
32 R. I. Kureshy, I. Ahmad, N. H. Khan, S. H. R. Abdi, S. Singh, P. H. Pandia and R. V. Jasra, *J. Catal.*, 2005, **235**, 28–34.
33 R. Schmidt, E. W. Hansen, M. Stoecker, D. Akporiaye and O. H. Ellestad, *J. Am. Chem. Soc.*, 1995, **117**, 4049–4056.
34 D. Zhao, J. Zhao, S. Zhao and W. Wang, *J. Inorg. Organomet. Polym.*, 2007, **17**, 653–659.
35 S. Zolezzi, E. Spodine and A. Decinti, *Polyhedron*, 2002, **21**, 55–59.
36 V. S. Chan, M. Chiu, R. G. Bergman and F. D. Toste, *J. Am. Chem. Soc.*, 2009, **131**, 6021–6032.
37 P. Yan, Y. Sugiyama, Y. Takahashi, H. Kinemuchi, T. Temma and S. Habaue, *Tetrahedron*, 2008, **64**, 4325–4331.
38 S. Takizawa, T. Katayama and H. Sasai, *Chem. Commun.*, 2008, 4113–4122.